11^{th} International Conference on Fracture Mechanics of Concrete and Concrete Structures
FraMCoS-11
J. M. Chandra Kishen, A. Ramaswamy, S. Ray and R. Vidyasagar (Eds)
https://doi.org/10.21012/FC11.092398

A COMPARATIVE STUDY OF IMPLICIT AND EXPLICIT SOLUTION PROCEDURES FOR COMPUTATIONAL MODELING OF REINFORCED CONCRETE STRUCTURES

NIELS W. KOSTENSE*, YUGUANG YANG*, MAX A.N. HENDRIKS*† AND JAN G. ROTS*

*Delft University of Technology
Delft, The Netherlands
e-mail: n.w.kostense@tudelft.nl

†Norwegian University of Science and Technology
Trondheim, Norway

Key words: Reinforced concrete; Numerical analysis; Solution procedures; Shear failure, Computational modeling strategies

Abstract. This paper presents a systematic comparison between implicit and explicit solution procedures for simulating the fracture processes in reinforced concrete. Implicit procedures are known to suffer from convergence problems due to negative softening stiffness, bifurcations and snap-backs. Explicit techniques have the potential to overcome those, but examples are rather scarce. In this study a popular total-strain based constitutive crack-crush model has been implemented in an explicit framework and consistent comparisons are made between the explicit and implicit solution procedures. Using identical finite element discretization and the same constitutive model, a range of benchmarks tests has been analyzed, including single element tests, a notched beam, a shear panel, and a shear critical RC beam. The results indicate that the explicit procedure could serve as a viable and robust alternative to the implicit approach, particularly in scenarios with highly brittle failure modes. As a side topic, it was found that the rotating format of the smeared crack model may produce over-rotation of cracks towards the direction of the rebars, rather than keeping them orthogonal to the rebars, as compared to a fixed crack format, for both the explicit and implicit approach.

1 INTRODUCTION

Non-Linear Finite Element Analysis (NLFEA) is becoming an increasingly popular modeling approach for the safety assessment of reinforced and prestressed concrete structures. However, their softening behavior and brittle failure modes pose significant challenges from a computational point of view. In many cases, the crack and crush propagations under progressive loading can exhibit bifurcation points, snap backs, and snap-throughs, which may lead to unstable and even inaccurate numerical results. To this end, conventional implicit incremental-iterative solution procedures such as Newton-Raphson have been enriched by various improvements such as arc-length methods and indirect displacement control methods. Nevertheless, when analyzing real-scale RC structures with multiple fracture localizations, convergence of the incremental-iterative procedures cannot

always be achieved, especially beyond local peaks or global peaks in the load displacement response.

In an effort to circumvent these stability issues, the sequentially linear solution procedure [1] has been proposed and successfully employed at structural level by e.g. Slobbe et al. [2]. An alternative is to use an explicit solver, which is a time-based approach that simulates the unstable fracture process dynamically rather than trying to capture it statically with path-following techniques. Although implicit incremental-iterative techniques are still common practice amongst structural engineers, it is worth evaluating the performance of an explicit solver. However, consistent comparative studies between implicit and explicit solution procedures have so far been carried out only to a limited extent, e.g. [3]. This is mainly due to the fact that explicit analyses come with increased computational costs and the available constitutive models are often geared towards high-dynamic events involving high strain rates. Consequently, static features such as the reduction in compression capacity due to lateral cracking have received less attention in these explicit models. In this study, a fully featured total-strain based smeared crack/crush model, available in an implicit FEM framework, has been re-formulated and implemented in an explicit FEM framework. Subsequently, a set of benchmarks is analyzed using both the explicit and implicit solution technique while adopting the same constitutive model and finite element discretization.

2 METHODOLGY

2.1 Finite element discretization

In this study, we limit ourselves to a 2D plane stress configuration. The element size is varied depending on the requirements of the selected problem, ranging from 10 mm to 125 mm.All the analyses are performed with a uniform mesh consisting of linear quadrilateral elements with full 2 x 2 Gauss integration. The reinforcement is modelled with simple truss elements, letting the nodes of the truss elements coincide with the nodes of the quadrilateral elements, assuming perfect bond.

2.2 Constitutive model

The model presumes that incipient cracking occurs perpendicular to the direction of maximum principal strain, as illustrated fig. 1a, by the introduction of the crack or n,t-coordinate system. The routine is commenced by computing the total strain vector $\boldsymbol{\varepsilon_{xy}}$ in the global x,y-coordinate system, followed by a transformation of the strains to the n,t-coordinate system. In the implicit solution procedure, this strain vector is update each iteration and in the explicit solution procedure entering each timestep. After the computation of the total strain vector, the angle of the principal strain direction is determined as

$$\tan(2\theta_\varepsilon) = \frac{\gamma_{\mathrm{xy}}}{\varepsilon_{\mathrm{xx}} - \varepsilon_{\mathrm{yy}}} \tag{1}$$

and is subsequently used to transform the total strain vector to the crack n,t-coordinate system according to the transformation matrix $\boldsymbol{T}_\varepsilon(\theta)$,

$$\boldsymbol{\varepsilon}_{nt} = \boldsymbol{T}_\varepsilon(\theta_\varepsilon)\boldsymbol{\varepsilon}_{xy} \tag{2}$$

In order to employ the uni-axial stress-strain laws defined in the n,t-coordinate system, the strain vector is multiplied by a projection matrix P resulting in an equivalent uni-axial strain vector defined as

$$\tilde{\varepsilon}_{\mathrm{nt}} = \boldsymbol{P}\boldsymbol{\varepsilon}_{\mathrm{nt}} \tag{3}$$

where $\boldsymbol{P}$ is the projection matrix, which is defined as:

$$\mathbf{P} = \frac{1}{1-\nu_{\mathrm{nt}}\nu_{\mathrm{tn}}} \begin{bmatrix} 1 & \nu_{\mathrm{nt}} & 0 \\ \nu_{\mathrm{tn}} & 1 & 0 \\ 0 & 0 & 1-\nu_{\mathrm{nt}}\nu_{\mathrm{tn}} \end{bmatrix} \tag{4}$$

where ν_{nt} and ν_{tn} are reduced values of the Poisson ratios in the n,t-coordinate system.

Within the n,t-coordinate system, the constitutive model is then formulated as a function of the equivalent strain vector $\tilde{\boldsymbol{\varepsilon}}_{\boldsymbol{nt}}$ as

$$\boldsymbol{\sigma_{nt}} = \sigma(\tilde{\boldsymbol{\varepsilon}}_{nt}) \tag{5}$$

Once the stresses in the n,t-coordinate system have been computed, the stresses are transformed back again to the global x,y-coordinate system,

$$\boldsymbol{\sigma}_{xy} = \boldsymbol{T}_{\sigma}(\theta_{\varepsilon})\boldsymbol{\sigma}_{nt} \tag{6}$$

where $\boldsymbol{T}_{\sigma}(\theta_{\varepsilon})$ is the transformation matrix for the stress vector and $\boldsymbol{\sigma}_{nt}$ is the stress vector in the crack n,t-coordinate system. Note that the fixed and rotating formulations coexist within the same framework, where the transformation matrix is kept constant in the post-cracking stage within a fixed crack formulation and is continuously updated maintaining coaxiality between principal stress and principal strain in the case of a rotating crack formulation.

Within the constitutive framework as described above, the following features are deployed:

- Tension softening is described by a fracture energy based exponential stress-strain relationship, based on work of Hordijk et al. [4], and presented in fig. 1b.
- The compression softening curve is based on a parabolic relation as proposed by Feenstra et al. [5] and is shown in fig. 1c.
- The crack band width is estimated using the projection method proposed by Govindjee et al. [6].
- In the fixed crack formulation, a damage based shear retention factor is applied to account for the shear stresses perpendicular to the crack plane [7].
- Reduction of the compressive strength due to lateral cracking is applied according to Vecchio et al. [8].

2.3 Solution procedures

Nonlinear static problems are traditionally solved using an implicit solution procedure. Typically, an incremental-iterative scheme like the Newton-Raphson method is used to solve the nonlinear equilibrium equations. The accuracy is controlled by convergence criteria expressed via displacement, force and/or energy norms. Although this method is proven to be effective in many cases, stability issues may arise in the case of different suddenly emerging sources of nonlinear behavior. In the implicit analysis presented in this study, a regular Newton-Raphson incremental iterative procedure is adopted with convergence criteria based on force or displacement tolerance of 1%.

Explicit solution procedures serves as an alternative to the conventional implicit solution method. However, it is typically not the preferred choice due to several disadvantages, including its higher computational demand. The explicit approach employs the central difference method, which is conditionally stable and necessitates careful consideration of critical time step size to ensure numerical stability. To reduce analysis time, strategies like time scaling or mass scaling can be applied. A distinctive advantage of the explicit approach is its ability to avoid convergence issues and the requirement for static equilibrium, simplifying the analysis process. For efficiency reasons, it is particularly inclined towards utilizing reduced integration and a diagonal mass matrix. Additionally, damping techniques, both global and frequency-dependent, can be incorporated to enhance stability. This methodology involves a quasi-static analysis approach and is consequently loading rate dependent. To verify the quasi-static equilibrium, internal and kinetic energy considerations as well as force imbalances (external and reaction forces) can be examined.

Some practical considerations have to be taken into account regarding the utilization

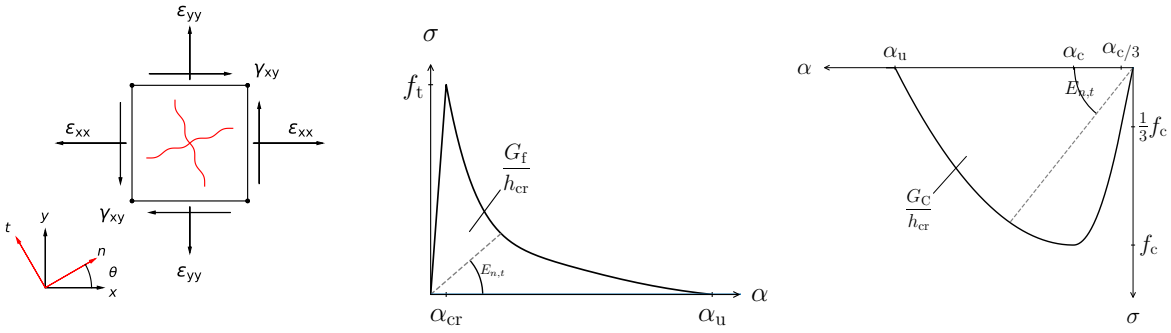

(a) Crack coordinate system (b) Tension softening [4] (c) Compression softening [5]

Figure 1: Total strain based smeared crack model

of the explicit solution procedure. The critical time step is directly related to the element size implying that a mesh refinement has severe consequences on the analysis time, hence an optimal element size has to be chosen that is sufficiently small to capture the relevant physical phenomena, but sufficiently large to ensure a reasonable analysis time. The critical time step size is defined as:

$$\Delta t_{\mathrm{cr}} = \alpha \frac{l}{c} \tag{7}$$

where α is a constant that adds additional margin to the critical time step size and is often taken as $\alpha = 0.9$, l is the element size and c is the wave speed. The wave speed is calculated for 2D continuum and 1D elements as:

$$c_{\mathrm{2D}} = \sqrt{\frac{E}{(1-\nu)\rho}}, c_{\mathrm{1D}} = \sqrt{\frac{E}{\rho}} \tag{8}$$

Under the assumption that the analysis time scales linearly with the number of elements and the adopted time increment, a mesh refinement of a factor 2 will increase the analysis time by a factor 8 in a 2D model and by a factor 16 in a 3D model. For concrete modelled with an element size in the range of $l = 25 - 200\,\mathrm{mm}$, a Young's modulus of $E = 30000 - 38000\,\mathrm{MPa}$, a Poisson's ratio of $\nu = 0.15$ and a density of $\rho = 2400\,\mathrm{kg/m^3}$, the critical time step can be expected to be in the range of $\Delta t_{\mathrm{cr}} = 5\,\mu\mathrm{s} - 50\,\mu\mathrm{s}$.

3 VALIDATION AT ELEMENT LEVEL

This single element test serves as a preliminary analysis for the comparison of the implicit and explicit solution procedures on structural level. The primary objective is to verify the equivalence of the constitutive models under controlled loading conditions. Besides this, additional insight is given into the physical significance by employing a fixed or rotating crack formulation, which goes back to the early days of the smeared crack approach [9] and is still a topic of debate [10].

A variety of single element tests is performed, although we restricts ourselves to the tension-shear problem, as it is most relevant for the description of the combined cracking and shearing behavior. The tension-shear problem is inspired by [11], where the material input parameters and dimensions are modified to comply with elements used on a structural level. The analysis is performed on a four nodes quadrilateral plane stress element with a size of 100 x 100 mm^2 and a thickness of 100 mm. The adopted material properties are presented in section 3. The element is subjected to non-proportional loading as visualized in fig. 2 considering two loading stages:

- Loading Stage A: Uni-axiale tensile strain load $\Delta\varepsilon_{\mathrm{xx}} = \varepsilon_{\mathrm{cr}}$ where the crack is initiated perpendicular to the x-direction. Lateral effects in the y-

direction are suppressed by the addition of a strain load in y-direction of $\Delta\varepsilon_{yy} = -\nu_0\varepsilon_{xx}$.

- Loading Stage B: A bi-axiale tensile strain load combined with a shear strain load with ratio of $\Delta\varepsilon_{xx} : \Delta\varepsilon_{yy} : \Delta\gamma_{xy} = 0.5 : 0.75 : 1$

By the applied strain load, the inertia effects are eliminated, making the response in terms of stress-strain relationship solely dependent on the constitutive law. In fig. 3 the crack patterns of the single element test are presented at integration point level, where fig. 5 and fig. 4 show the stress-strain relationship for the Rotating and Fixed crack formulation respectively. It is observed that the stress-strain diagrams are identical for both solution procedures. Only a small deviation is observed in the softening branch of the stress-strain diagrams, which is subscribed to the difference in step size. The damage based reduction of the Poisson ratio is based upon the damage obtained from the previous load or timestep. Reducing the step size of the implicit solution procedure would make the stress strain diagrams converge to the same solution as for the explicit solution procedure. As the crack in the fixed crack formulation evolves, the orientation remains fixed and eventually a second crack is initiated in the y-direction. By letting the n,t-coordinate system coincide with the global coordinate system, the strain softening as defines by the softening law is reflected by the stress-strain diagrams fig. 5a and fig. 5b. As damage propagates in the crack normal direction, the damage-based shear retention factor is scaled down with the same rate. Consequently, the shear stiffness is reduced to zero once the ε_{yy} reaches ε_u, defining the end of the softening branch. The rotating crack formulation shows a substantially different behavior where the crack rotates and coincides with the pricipal strain directions. In addition, the crack bandwidth is now dependent on the crack direction, which also determines the shape of the softening curve. Both features make the interpretation of the stress-strain relationships not straightforward and ask for a detailed elaboration, which goes beyond the intention of this paper.

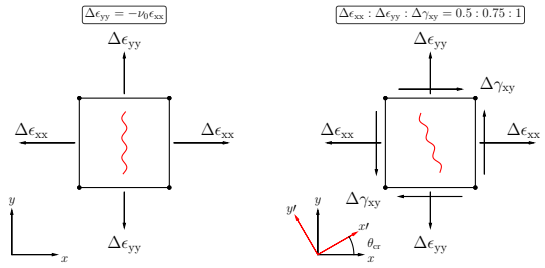

(a) Loading stage 1 (b) Loading stage 2

Figure 2: Tension-shear problem

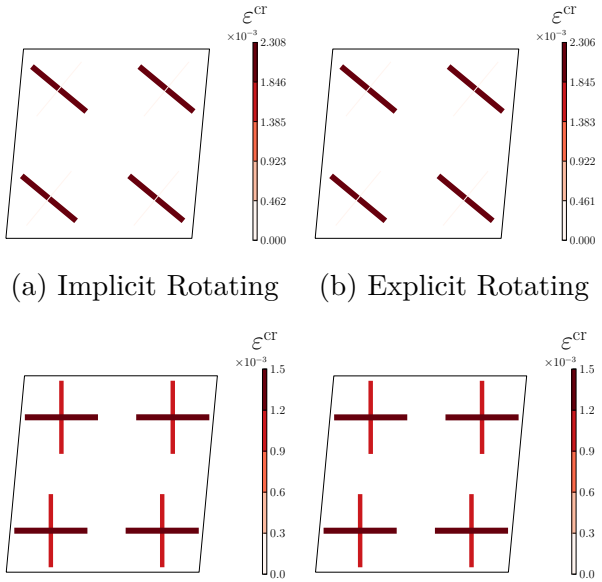

(a) Implicit Rotating (b) Explicit Rotating

(c) Implicit Fixed (d) Explicit Fixed

Figure 3: Tension-shear test: Crack strains ϵ_{cr}

4 COMPARISON CASE STUDIES AT STRUCTURAL LEVEL

After gaining confidence in the implemented constitutive model, the model is applied to a series of case studies on a structural level.

Table 1: Overview of adopted concrete material properties in case-studies

Parameter	Tension-shear	Notched beam C2B1	Shear-panel	Shear beam S1B1	Units
E_0	30000	33500	30000	33551	N/mm^2
f_t	3.0	3.1	3.0	3.5	N/mm^2
G_f^I	100	160	100	76.5	N/mm
ν_0	0.15	0.15	0.15	0.15	-

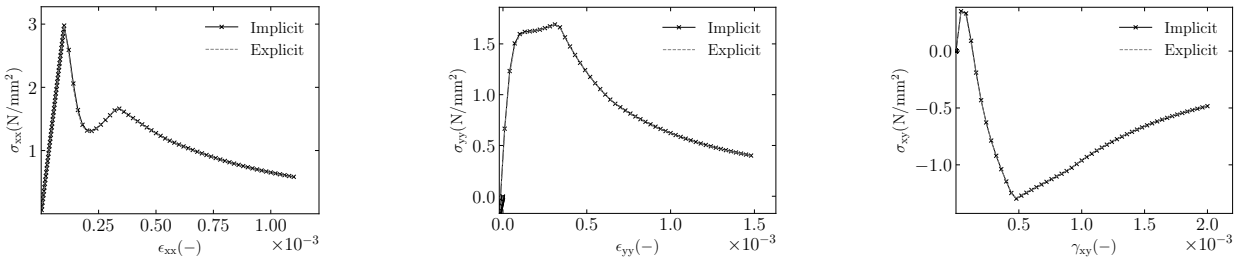

(a) ε_{xx} - σ_{xx} (b) ε_{yy} - σ_{yy} (c) γ_{xy} - σ_{xy}

Figure 4: Tension-shear test: Rotating crack orientation

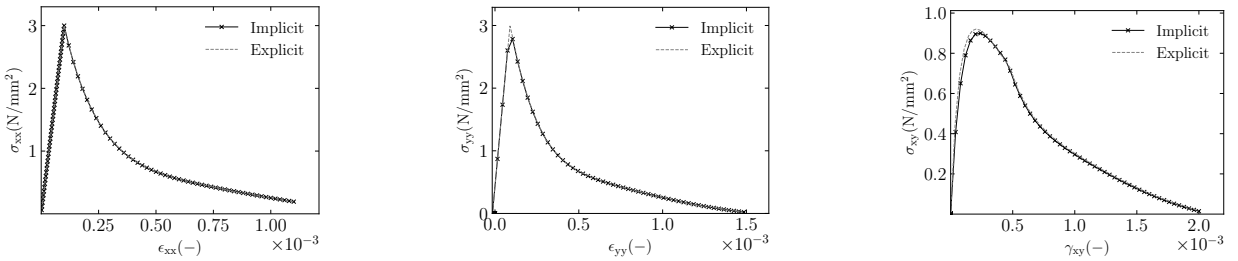

(a) ε_{xx} - σ_{xx} (b) ε_{yy} - σ_{yy} (c) γ_{xy} - σ_{xy}

Figure 5: Tension-shear test: Fixed crack orientation

4.1 Notched beam

Firstly, a simple benchmark of a 3-point bending test of an unreinforced notched beam is considered, conducted by Sarkhosh [12]. The specimen's dimensions (l x b x h) are 1000 x 125 x 125 mm^3, featuring a notch with a depth of 40 mm, fig. 6. The material properties of the concrete are summarized in section 3. With respect to the applied loading, in the implicit solution procedure, a displacement controlled load is defined with displacement increments of $\Delta u =$ 0.01mm. In similar fashion, for the explicit solution procedure, a constant velocity-controlled load is applied, with a loading rate of $\dot{u}_y = 1.0$mm/s. Notably, to minimize inertia effects, the velocity is gradually increased within a timeframe of $\Delta t = 0.1$s. The finite element mesh is discretized with an average element size of 10 x 10 mm^2. The load-displacement response of the implicit and explicit solution procedure are shown in fig. 7, both for the fixed and rotating crack orientation. In accordance with the adopted softening relation, an exponential softening behavior is obtained for both the implicit and explicit solution procedure. When comparing the load deflection curves of the implicit and explicit solution procedure, it is observed that the structural response of the implicit solution procedure is slightly more brittle than for the explicit solution proce-

dure, but the difference is only marginal. For this symmetric case with a vertical crack, we do not observe a difference between the use of a rotating or fixed crack concept, for both the explicit and implicit procedure, as illustrated in fig. 7 for the load-displacement response and fig. 8 for the crack pattern. The conclusion is that this proportionally loaded mode-I single fracture test can both be handled well and stable by implicit and explicit procedures.

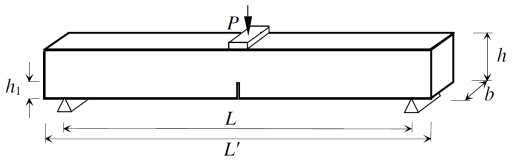

Figure 6: Notched beam, taken from [12].

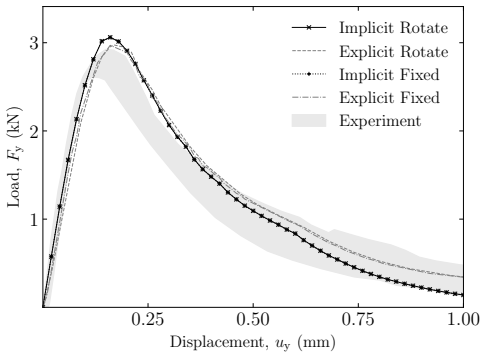

Figure 7: Load-deflection of notched beam.

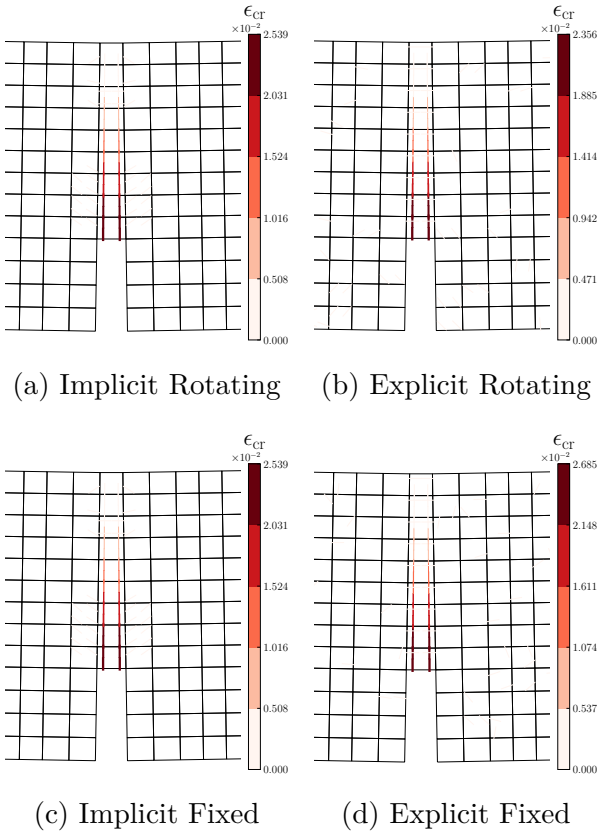

(a) Implicit Rotating (b) Explicit Rotating

(c) Implicit Fixed (d) Explicit Fixed

Figure 8: Notched beam: Crack strains ε_{cr}

4.2 Shear panel under non-proportional loading

Due to the authors specific interest in the computational modelling of prestressed concrete beams, the next case study concerns a nonproportional loading case, for a fictitious shear panel. Here the same principle is followed as for the tension shear problem from section section 3; now the panel is initially preloaded in compression and subsequently in shear. The analysis mimics a more brittle kind of failure mechanism, similar to diagonal tension failure in the web of a prestressed concrete beam without shear reinforcement. As no experiment is available, the case just serves for mutual comparisons between implicit and explicit procedures. The shear panel is unreinforced and has a size of 1000 x 1000 mm and a thickness of 100 mm. The material properties of the concrete are the same as for the single element tests presented in section 3. The prestressing is modelled

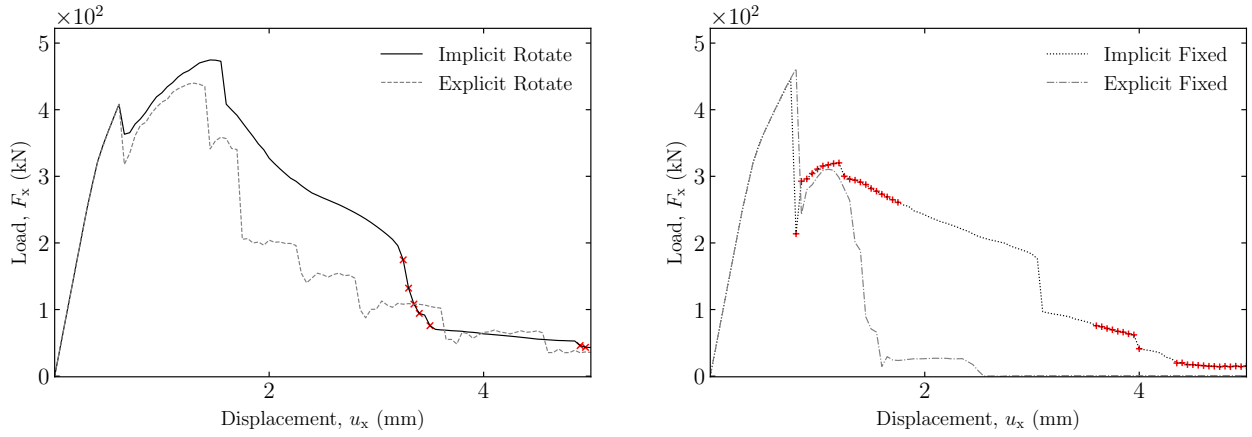

(a) Rotating (b) Fixed

Figure 9: Load-displacement diagrams of shear panel under non-proportional loading. Red markers indicate non-converged steps for the implicit FEM analysis.

by a compressive stress of $\sigma_{cp} = 6\text{N/mm}^2$ and is applied as a prescribed deformation load in the y direction. The geometry is subdivided into 8 elements, resulting in an element size of 125 x 125 mm^2. The load-displacement curves are presented in fig. 9a and fig. 9b for the rotating and fixed format respectively. The red markers indicate the load steps that are not fully converged in the implicit analysis. In terms of load-displacement response, the explicit models are more brittle compared to the implicit analysis. Comparing the crack pattern of the implicit and explicit solution procedure for the rotating crack formulation fig. 10, it is noted that the crack strain magnitude of the explicit results is slightly larger than for the implicit results. Conversely, the crack bandwidth, in this context meaning the area of the elements whereover the diagonal crack is distributed, is slightly narrower in the explicit analysis. In other words, the crack pattern of the explicit solution procedure tends to localize more than for the implicit solution procedure. The lack of convergence for the implicit procedure obviously results in a less sharp and irregular localization, and a too high residual post-peak branch for the implicit procedure, as compared to the explicit procedure which has no problem in following the steep structural softening down to zero.

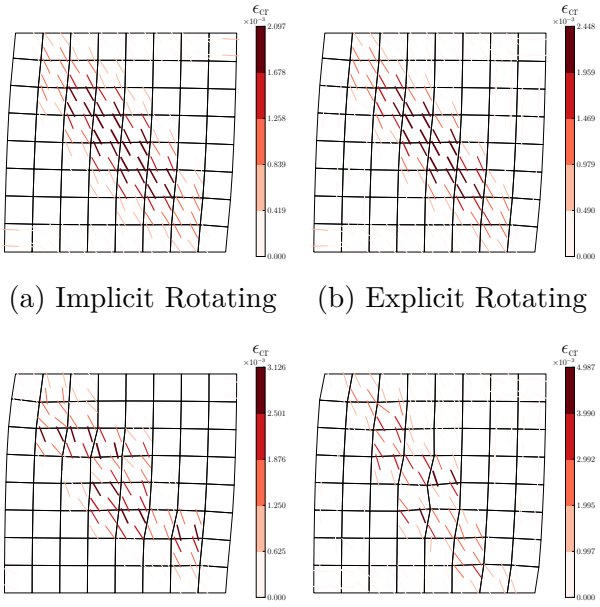

(a) Implicit Rotating (b) Explicit Rotating

(c) Implicit Fixed (d) Explicit Fixed

Figure 10: Crack patterns of shear panel under non-proportional loading ($\Delta u_x = 2\text{mm}$).

4.3 Shear critical RC beam

The final case study entails a shear critical reinforced concrete (RC) beam without shear reinforcement, again taken from the experimental campaign conducted by Sarkhosh

et al. [12]. Such a shear critical beam is notorious for its brittle failure mode, from which the physical behavior is known to be quite challenging to capture with conventional implicit solution procedures. This is illustrated in fig. 12, which depicts the experimentally obtained failure indicating sudden brittleness, where shear failure is established within a time interval of $\Delta t = 0.01$s. The experimental program encompassed seven distinct series of beams, designed to analyze both short-term and long-term influences on shear resistance. For our analysis, we focus on the first series, which exclusively comprises short-term tests involving six identical specimens, denoted as S1B1 to S1B6. The beams are subjected to 3-point bending configuration, possess dimensions of 3000 x 450 x 200 mm^3 and incorporate three longitudinal reinforcement bars, each with a diameter of 20 mm. The effective span of the beam measures 2400 mm, yielding a shear span-to-depth ratio of 2.93. To avoid anchorage failure, anchoring plates are affixed to the longitudinal reinforcing bars at the bottom of the beam, securely fastened at both ends. The dimensions and reinforcement details of the beam are presented in fig. 11. To characterize the material properties of the concrete, we rely upon data from experimental investigations, and these properties are displayed in section 3. The finite element model is discretized with a uniform mesh with an average element size of 20 x 20 mm^2 elements, resulting in 23 elements over the height of the beam. The reinforcement is modelled with simple truss elements under the assumption of perfect bond, letting the nodes of the truss elements coincide with the nodes of the concrete. As no yielding of the reinforcement is expected, the truss elements are modelled with a linear elastic constitutive law, with a Young's modulus of $E = 200000\text{N/mm}^2$ and a cross sectional area of $A_\text{s} = 942\text{mm}^2$. As in the preceding case studies, the loading protocol remains consistent, applying a constant velocity-controlled load within the explicit solution framework.

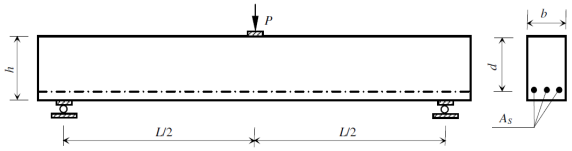

Figure 11: Shear critical RC beam, taken from [12].

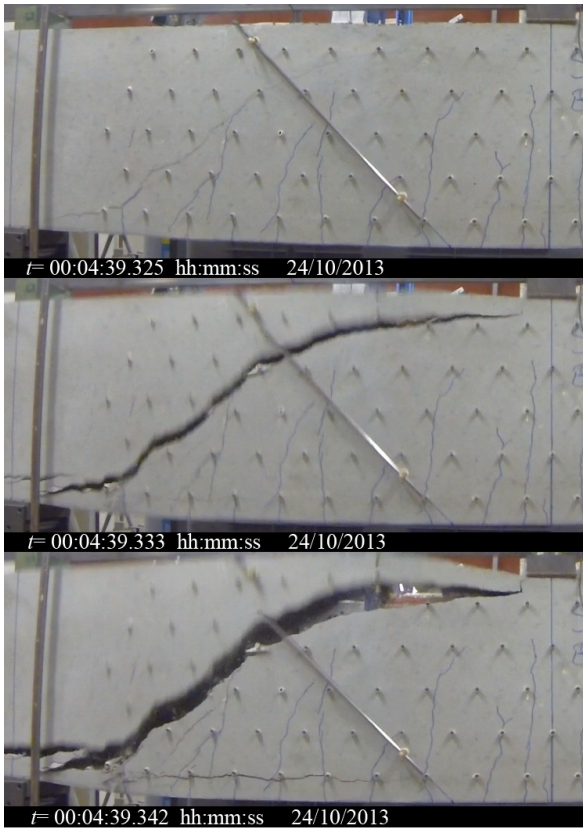

Figure 12: Shear critical RC beam within $\Delta t = 0.01$s, taken from [12].

The outcomes of the fixed crack formulation are depicted in fig. 14c and fig. 14b for the implicit and explicit analysis respectively, showcasing the crack pattern right after the ultimate load values has been reached. Both the implicit and explicit analysis yield comparable and realistic crack patterns, aligning closely with the experimental observations. It is worth highlighting that the crack pattern discerned through the explicit solution procedure exhibits a

stronger resemblance to the experimental observations. This close correspondence underscores the fidelity of the explicit solution method in capturing the intricate behavior of the shear critical RC beam under investigation. The load-displacement diagrams stemming from the fixed crack formulation are depicted in fig. 13b. They represent the experimental maximum load accurately, where the implicit solution procedure yields a slightly higher peak load than the explicit solution procedure. Another outstanding difference is observed in the post-peak trajectory. In the explicit analysis, the load drops to zero, whereas in the implicit analysis, it continues with another rising branch. The post-peak load trajectory in the implicit analysis is accompanied by a large number of non-converged load-steps, which renders the results unreliable. Evidently, the explicit analysis does not suffer from such convergence issues.

Findings from the analysis of the rotating crack formulation for the implicit fig. 14a and explicit fig. 14b frameworks reveal a peculiar behavior in terms of crack pattern. Remarkably, a distinctive crack pattern emerges, exhibiting certain characteristics that deviate from physical expectations. The observed crack pattern is best described as a delamination of the concrete layer below the reinforcement. This phenomenon is attributed to the excessive rotation of the crack beyond reasonable limits, tending to align it with the rebar direction, rather than keeping the cracks orthogonal to the rebar. In a previous study similar over-rotation of cracks was reported [13]. This over-rotation emerges in specific situations and is qualified as a deficiency of the rotating crack formulation. The results indicate once again that the choice of the crack formulation should not be taken lightly and can be a decisive factor in the accuracy of the analysis. Following the non-physical nature of the crack pattern obtained with the rotating crack formulation, the load-displacement diagram is for completeness given in fig. 13a. We observe that the peak load is far too low, and a residual rising branch is found which cannot be explained from physical reasoning as dowel effects have been excluded from the analysis.

5 DISCUSSION AND CONCLUSIONS

As we conclude this exploration study between implicit and explicit solution procedure, several key takeaways are pointed out.

1. A total strain based smeared crack model has implemented within an explicit framework for the first time. With the implemented constitutive model in place, the explicit solution procedure is capable running the analysis without any stability issues, were the implicit solution procedure is suffering from non-converged load steps.

2. With the adopted constitutive model, the implicit and explicit solution procedure show equivalent results for the single element tests. Only a minor difference is observed in the softening behaviour of the single element tests, which is subscribed to the smaller step size of the explicit solution procedure. The Poisson ratio is scaled proportional to the damage variable, which is for efficiency reasons taken from the previous load step.

3. The explicit solution procedure is capable of capturing the structural response of the chosen benchmark problems. By applying an appropriate load rate, a quasi-static response could be obtained, which can be verified by monitoring the kinetic energy of the system and the out-of-balance reaction forces.

4. When encountering rapid crack development in structural response leading to highly brittle failure, the explicit solution method proves its capa-

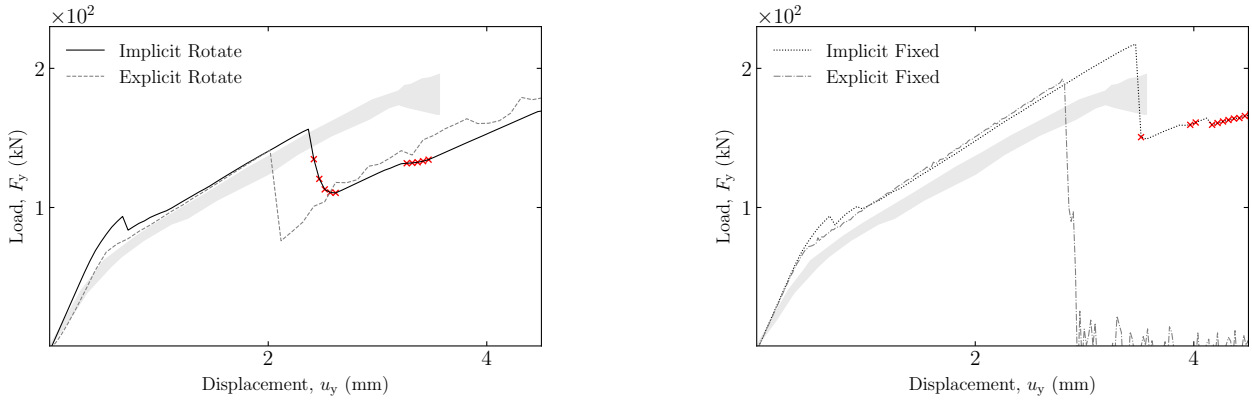

(a) Rotating

(b) Fixed

Figure 13: Load displacement diagram of analysis of shear critical RC beam under 3-point bending

bility to promptly capture these significant changes due to the small adopted timestep. This phenomenon becomes apparent when examining the benchmarks of the shear critical RC beam. Here, the governing crack emerges within a very short timeframe, making it hard to capture by an implicit schema. The explicit solution method emerges as a feasible alternative in scenarios characterized by sudden shifts in the dominant crack pattern, showcasing its potential to outperform the implicit method in such circumstances.

5. The rotating crack orientation is found to suffer from over-rotating cracks due to excessive rotation of the crack beyond reasonable limits, tending to align it with the rebar direction, rather than keeping the cracks orthogonal to the rebar. This observation is in line with the findings of [13], where the rotating crack orientation is found to be less suitable for the modelling of RC beams without shear reinforcement.

REFERENCES

[1] J. G. Rots. Sequentially linear continuum model for concrete fracture. Fracture mechanics of concrete structures, 13:831–839, 2001.

[2] Hendriks M. A. N. Rots J. G. Slobbe, A. T. Sequentially linear analysis of shear critical reinforced concrete beams without shear reinforcement. Finite Elements in Analysis and Design, 50:108–124, 2012.

[3] Yang Y. Wang J. J. Fan J. S. Tao M. X. Mo Y. L. Liu, C. Biaxial reinforced concrete constitutive models for implicit and explicit solvers with reduced mesh sensitivity. Engineering Structures, 219:110880, 2020.

[4] D. A. Hordijk. Local approach to fatigue of concrete. 1993.

[5] P. H. Feenstra. Computational aspects of biaxial stress in plain and reinforced concrete. PhD thesis, Delft University of Technology, 1993.

[6] Kay G. J. Simo J. C. Govindjee, S. Anisotropic modelling and numerical simulation of brittle damage in concrete. International journal for numerical methods in engineering, 38(21):3611–3633, 1995.

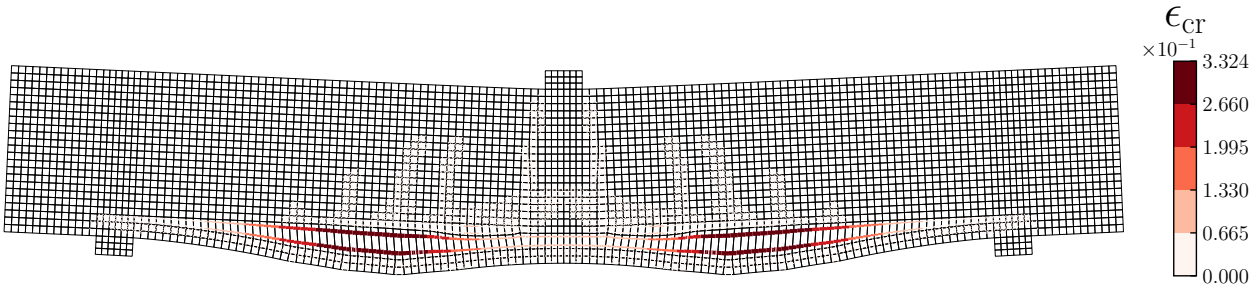

(a) Implicit - Rotating

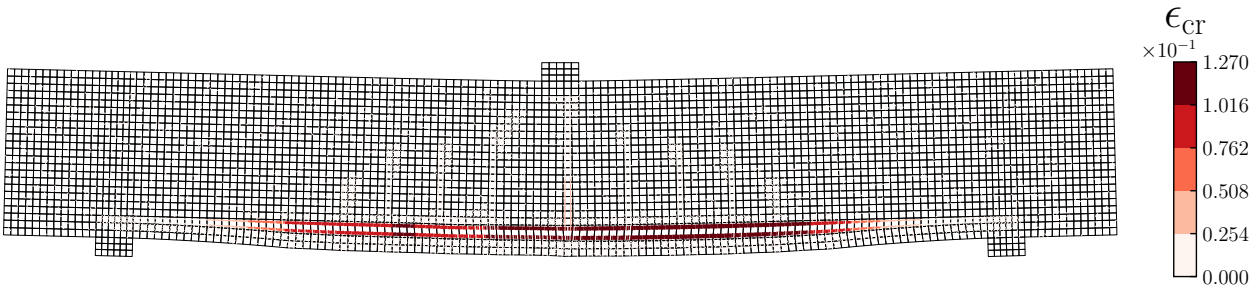

(b) Explicit - Rotating

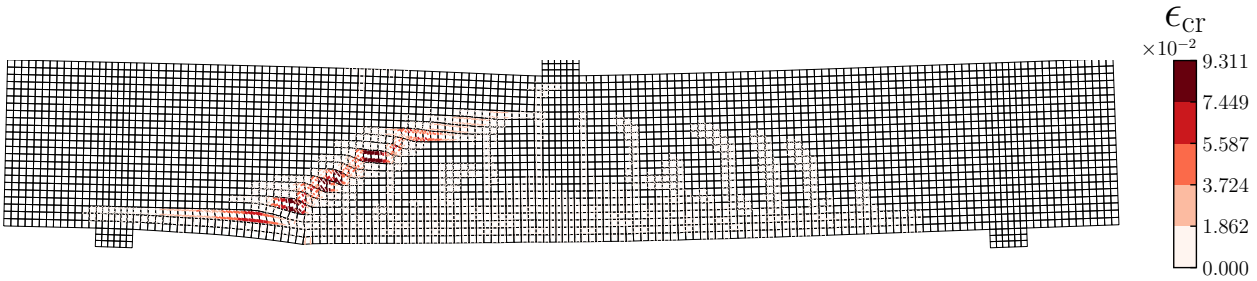

(c) Implicit - Fixed

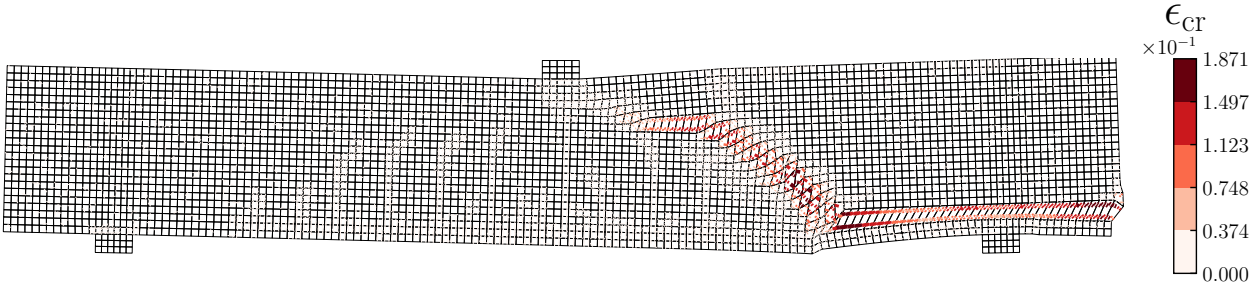

(d) Explicit - Fixed

Figure 14: Crack pattern of shear critical RC beam under 3-point bending

[7] Hendriks M. A. N. Rots J. G. DeJong, M. J. Sequentially linear analysis of fracture under non-proportional loading. Engineering Fracture Mechanics, 75(18):5042–5056, 2008.

[8] Collins M. P. Vecchio, F. J. Compression response of cracked reinforced con-

crete. Journal of structural engineering, 119(12):3590–3610, 1993.

[9] Blaauwendraad J. Rots, J. G. Crack models for concrete, discrete or smeared? fixed, multi-directional or rotating? HERON, 34 (1), 1989, 1989.

[10] Hendriks M. A. N. Rots J. G. Yang Y. Engen M. van den Bos A. A. de Putter, A. Quantification of the resistance modeling uncertainty of 19 alternative 2d nonlinear finite element approaches benchmarked against 101 experiments on reinforced concrete beams. Structural Concrete, 23(5):2895–2909, 2022.

[11] Pramono E. Sture S. Willam, K. Fundamental issues of smeared crack models. In Fracture of Concrete and Rock: SEM-RILEM International Conference June 17–19, 1987, Houston, Texas, USA, pages 142–157. Springer, 1989.

[12] R. Sarkhosh. Shear Resistance of Reinforced Concrete Beams without Shear Reinforcement under Sustained Loading. PhD thesis, 2014.

[13] Hendriks M. A. N. Rots J. G. Yang Y. Engen M. van den Bos A. A. de Putter, A. Quantification of the resistance modeling uncertainty of 19 alternative 2d nonlinear finite element approaches benchmarked against 101 experiments on reinforced concrete beams. Structural Concrete, 23(5):2895–2909, 2022.